

PAPER • OPEN ACCESS

In vitro biocompatibility and electrical stability of thick-film platinum/gold alloy electrodes printed on alumina

To cite this article: Alejandro Carnicer-Lombarte *et al* 2017 *J. Neural Eng.* **14** 036012

View the [article online](#) for updates and enhancements.

Related content

- [Laser patterning of platinum electrodes for safe neurostimulation](#)
R A Green, P B Matteucci, C W D Dodds *et al.*
- [Performance of conducting polymer electrodes for stimulating neuroprosthetics](#)
R A Green, P B Matteucci, R T Hassarati *et al.*
- [Electrical stimulation promotes nerve cell differentiation on PPv/PMAS composites](#)
Xiao Liu, Kerry J Gilmore, Simon E Moulton *et al.*

Recent citations

- [Neuroprotective role of hyperforin on aluminum maltolate-induced oxidative damage and apoptosis in PC12 cells and SH-SY5Y cells](#)
Haoran Wang *et al*
- [Fabrication of Graphene Network in Alumina Ceramics with Adjustable Negative Permittivity by Spark Plasma Sintering](#)
Rui Yin *et al*



IOP | ebooks™

Bringing you innovative digital publishing with leading voices to create your essential collection of books in STEM research.

Start exploring the collection - download the first chapter of every title for free.

In vitro biocompatibility and electrical stability of thick-film platinum/gold alloy electrodes printed on alumina

Alejandro Carnicer-Lombarte^{1,4}, Henry T Lancashire^{2,4}
and Anne Vanhoestenberghé³

¹ John Van Geest Centre for Brain Repair, Department of Clinical Neurosciences, University of Cambridge, Cambridge, CB2 0PY, United Kingdom

² Centre for Materials Research, Department of Materials and Tissue, University College London, Stanmore, HA7 4LP, United Kingdom

³ Aspire Centre for Rehabilitation Engineering and Assistive Technology, Department of Materials and Tissue, University College London, Stanmore, HA7 4LP, United Kingdom

E-mail: a.vanhoest@ucl.ac.uk

Received 2 March 2017

Accepted for publication 8 March 2017

Published 30 March 2017



Abstract

Objective. High-density electrode arrays are a powerful tool in both clinical neuroscience and basic research. However, current manufacturing techniques require the use of specialised techniques and equipment, which are available to few labs. We have developed a high-density electrode array with customisable design, manufactured using simple printing techniques and with commercially available materials. **Approach.** Electrode arrays were manufactured by thick-film printing a platinum–gold alloy (Pt/Au) and an insulating dielectric on 96% alumina ceramic plates. Arrays were conditioned in serum and serum-free conditions, with and without 1 kHz, 200 μ A, charge balanced stimulation for up to 21 d. Array biocompatibility was assessed using an extract assay and a PC-12 cell contact assay. Electrode impedance, charge storage capacity and charge injection capacity were before and after array conditioning. **Main results.** The manufactured Pt/Au electrodes have a highly porous surface and exhibit electrical properties comparable to arrays manufactured using alternative techniques. Materials used in array manufacture were found to be non-toxic to L929 fibroblasts by extract assay, and neuronal-like PC-12 cells adhered and extended neurites on the array surfaces. Arrays remained functional after long-term delivery of electrical pulses while exposed to protein-rich environments. Charge storage capacities and charge injection capacities increased following stimulation accounted for by an increase in surface index (real surface area) observed by vertical scanning interferometry. Further, we observed accumulation of proteins at the electrode sites following conditioning in the presence of serum. **Significance.** This study demonstrates the *in vitro* biocompatibility of commercially available thick-film printing materials. The printing technique is both simple and versatile, with layouts readily modified to produce customized electrode arrays. Thick-film electrode arrays are an attractive tool that may be implemented for general tissue engineering and neuroscience research.

⁴ These authors contributed equally to this work.



Original content from this work may be used under the terms of the [Creative Commons Attribution 3.0 licence](https://creativecommons.org/licenses/by/3.0/). Any further distribution of this work must maintain attribution to the author(s) and the title of the work, journal citation and DOI.

Keywords: high-density electrode array, thick-film platinum electrodes, alumina ceramic, electrical stimulation, biocompatibility, *in vitro*

 Supplementary material for this article is available [online](#)

(Some figures may appear in colour only in the online journal)

1. Introduction

High-density electrode arrays are one of the most promising technologies at the interface of engineering and biology. By forming many independent electrical contacts with small subsets of cells, densely packed electrodes provide a unique tool to study the development and function of neural networks; whether *in vitro* or *in vivo* (Churchland *et al* 2007, Viventi *et al* 2011, Spira and Hai 2013). When used for electrical stimulation or recording purposes, this ‘high resolution’—in the order of hundreds to thousands of contact points per square centimetre—also holds great potential in the clinic. High-density arrays are being incorporated into visual prostheses, stimulating electrically smaller units within the retina to recreate a richer sensory experience in blind individuals (Palanker *et al* 2005, Sekirnjak *et al* 2008). Similar concepts are being designed to guide motor function in prosthetic limbs (Hochberg *et al* 2012, Collinger *et al* 2013) and to treat epilepsy (Waziri *et al* 2009).

Although high-density arrays are beginning to be implemented for a variety of applications, their widespread use is limited by challenges in their design and manufacture. Photolithography, wet etching, and thin-film deposition are the most common techniques used in the manufacture of these types of arrays (Borkholder *et al* 1997, Grumet *et al* 2000, Heuschkel *et al* 2002, Gholmieh *et al* 2006). Although these techniques do produce tightly packed circuits with micrometre-scale features, they involve multiple steps of production and require the use of specialized equipment and materials, which are rarely available to most neuroscience labs. Fabrication may be subcontracted, though we believe that the resulting gap between manufacture and biological testing may limit the widespread use of high-density electrode arrays. Another possible reason, especially applicable to reusable systems in biological testing labs, is their relative fragility and the challenge of interconnection. Therefore we find that there is, in the current research landscape, a need for alternative methods to produce high density electrode arrays.

Thick-film technology is amongst the simplest techniques used in circuit manufacturing. It is centred around the use of screen printing, in which an ink is transferred to a surface through a patterned screen. The pattern can be designed using standard drawing packages, no specialist software is required. In thick-film circuit manufacture, the inks used are special pastes which are dried then sintered to form electrically conductive or insulating features.

Thick-film printing is commonly used in many industries, the circuits are robust so it remains the preferred option for electronics operating in harsh environments (e.g. marine and

aerospace applications). Several well-established options for interconnection are available depending on the application. The versatility and low cost associated with this technique have made it the choice for areas of scientific research such as biosensor fabrication (Albareda-Sirvent *et al* 2000). This includes sensors for blood electrolytes (Pace and Hamerslag 1992), glucose (Bilitewski *et al* 1991), neuroactive compounds (Joshi *et al* 2005, Istamboulie *et al* 2010), and immuno-sensors (Wang *et al* 1998). Given the advantages presented, it would also be desirable to implement this technique in the field of neuroscience. We believe that for it to appeal to many researchers, we must demonstrate a high yield with electrode density in the hundreds per cm^2 using commercial manufacturing methods, so that any research lab could confidently subcontract the production to a local thick-film printing company. Cytotoxicity of commercially available pastes is therefore key to the adoption of the method, hence it is the focus of this paper. Further, electrode arrays can degrade and fail to function correctly with extended use, particularly when implanted within the body. We have therefore also tested the stability of thick-film arrays when exposed to a protein-rich environment, modelling long-term cell culture or implantation applications.

We have designed and produced an electrode array using thick-film printing techniques and commercially available base materials. The electrode sites, tracks, and connectors are composed of a single layer of platinum/gold (Pt/Au) alloy printed on an alumina ceramic plate. Insulation of tracks is achieved by printing a further layer of dielectric material on top. This process is well-established and produces circuits that are suitable for the long-term delivery of electrical pulses. Despite the simplicity of the manufacturing process, arrays can be produced with a high yield with an inter-electrode pitch of 500 μm , approximately equivalent to 400 electrode sites per cm^2 . Higher electrode densities, with a pitch of 75 μm , can be achieved using a laser to post-process the prints (Ordonez *et al* 2009). While this feature size is larger than that of some thin-film neural probes, we believe, for the reasons outlined previously, that the method will appeal to many researchers.

A potential major limitation in the use of commercial thick-film inks is biocompatibility, as the inks are designed for circuit manufacturing—and not for biological applications. However, we found none of the materials present in our arrays affected cell survival in *in vitro* cultures. Since electrode arrays have to be in close proximity with neurons to establish a successful interface, we tested the capacity of these cells to grow on our arrays as substrates. Neuronal-like cell lines were found to successfully attach and extend neurites; suggesting the thick-film arrays are suited for *in vitro* electrophysiological applications.

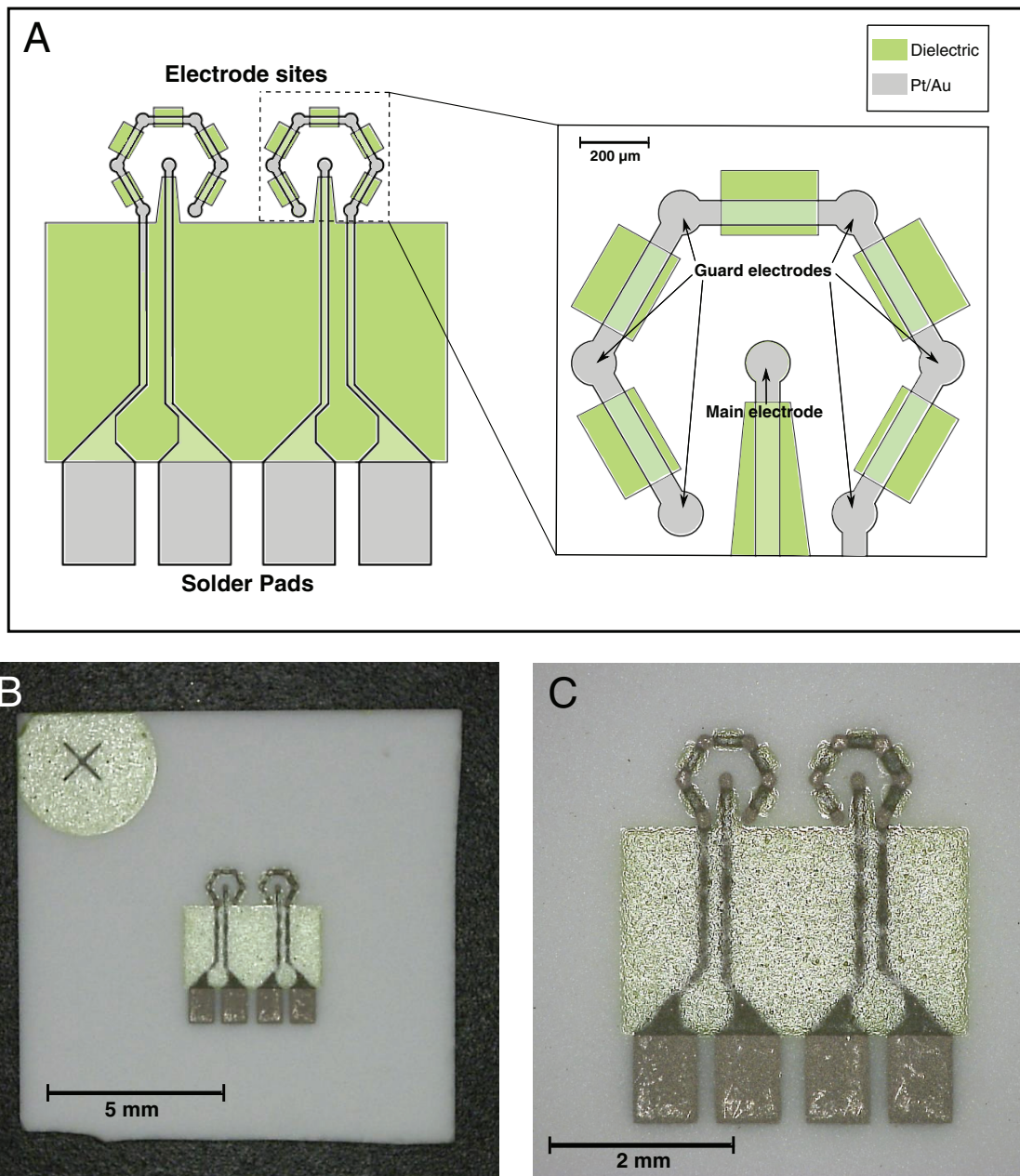


Figure 1. Hexagonal electrode array. (A) Diagram of the electrode array. The Pt/Au tracks (grey) are printed on top of the alumina plate (white background). Parts of the tracks are covered by a layer of dielectric (green) as a means of insulation. Each of the 14 electrode sites is designed to have an approximate diameter of 150 μm . (B) and (C) Optical images of the electrodes.

2. Materials and methods

2.1. Electrode array fabrication

Thick-film electrode arrays consisting of conductive Pt/Au tracks and insulating dielectric on alumina plates were manufactured by screen printing. Electrodes in the arrays were arranged in a hexagonal design: a main electrode surrounded by a ring of 6 electrically connected guard electrodes. Two hexagonal arrays were printed on each substrate. Schematic representation and optical micrographs of the hex electrode arrays are shown in figure 1. Although we chose to distribute the electrodes in hexagonal units for comparison with the

work of Green *et al* (2013), any other pattern could be produced with similar feature sizes.

To print the electrode arrays, patterns were designed using 2D-CAD software (AutoCAD, Autodesk Inc, and LibreCAD). Patterns were then either transferred onto homemade screens using a laser (Nd-YAG, Laservall Violino 2, Laservall) controlled by Smartist 4.1 software (Laservall), or sent to a subcontractor to produce professional quality screens (MCI Precision Screens). Pt/Au conductor paste (5837-G, ESL) was printed onto alumina plates (Rubalit, 708S, 96% Aluminium Oxide, CeramTec) through the screen, using a screen printing machine (model 1202, DEK). After levelling

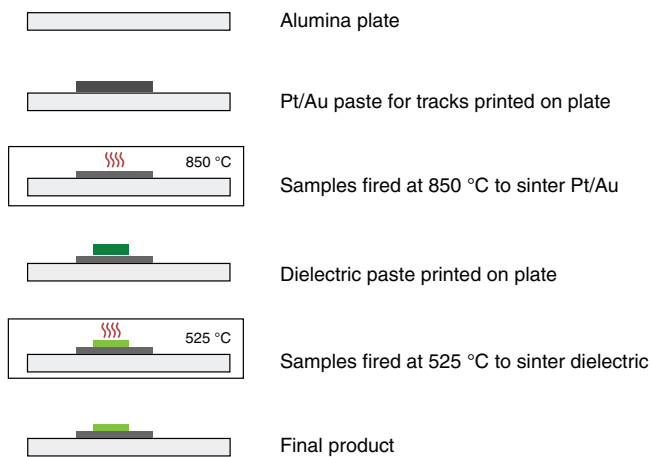


Figure 2. Summary of the fabrication process of a thick-film electrode array.

at room temperature for 5–10 min, the paste was dried at 125 °C for 15 min then fired at 850 °C for 10 min in a thick-film belt furnace (model 840, DEK). Dielectric paste (4771-p1, ESL) was printed on top of the plates, levelled and dried as the Pt/Au paste before sintering by firing at 525 °C for 5 min. The manufacturing process is summarized in figure 2.

When passing of electrical current through the electrode arrays was required, insulated tinned copper wires were soldered to the solder pads (figure 1). After thorough cleaning to remove flux residues, an insulating layer of silicone rubber (3140 RTV Coating, Dow Corning) was applied to the solder pads and cured at room temperature.

All electrode arrays were cleaned in detergent (Teepol-L, Teepol) and sodium phosphate solution, and rinsed in deionized water as previously described (Lonys *et al* 2015). Prior to the neuronal contact assay, electrode arrays were leached in ethanol (≥ 5 min), cleaned in acetone and steam autoclaved at 121 °C for 15 min.

2.2. Electrode array conditioning, including stimulation

To simulate long-term exposure to different environments, electrode arrays were placed for 3–21 d in plastic wells filled with phosphate-buffered saline (PBS), 100% foetal calf serum (FCS, heat inactivated, First Link Ltd), 1% horse serum diluted in culture medium (HS), or serum-free culture medium (SFCM). Culture medium composition is given in section 2.4.2. These arrays are referred to as conditioned electrode arrays. A group of each of these conditioned arrays also simultaneously underwent electrical stimulation to model charge transfer for extended periods of time. These arrays are referred to as Stimulated-Conditioned. Stimulation was in the form of a 1 kHz charge-balanced modified square wave with an amplitude of 220 μA and an interphase delay of 100 μs , delivered through a custom-made constant current circuit. Pulses were delivered between the central electrode (cathode) and the ring of grounded guard electrodes (anodes). The resultant cathodic charge per phase was 88 nC (a charge density of circa 0.3 mC cm^{-2} w.r.t. geometric area). These stimulation settings were recently used in an *in vitro* study of similarly proportioned electrode arrays to simulate long-term

passive degradation (Green *et al* 2013). The stimulation lasted for the entire conditioning phase, which, for 21 d, was equivalent to 1.8×10^9 pulses. Electrode array conditioning, including stimulation, is summarized in figures 3(a) and (b).

Conditioning lasted either 3 d in PBS, FCS, SFCM or HS (for the protein work, see section 2.5), or 21 d in PBS or 100% FCS (for the PC-12 cell culture, section 2.4.2), with medium changed every 7 d. Arrays conditioned for only 3 d are referred to as Short-Conditioned while the term Conditioned is used for the 21 d conditioning phase. This is illustrated by figures 3(a) and (b) respectively.

There were 4 groups that underwent the long conditioning phase: Conditioned-PBS, Stimulated-Conditioned-PBS, Conditioned-FCS and Stimulated-Conditioned-FCS (figure 3(a)). To these, a fifth group is added, the Unconditioned arrays. Some arrays of each of these 5 groups were removed at this stage for analysis (EIS, VSI and CV), the rest were used for PC-12 cell culture. The remaining arrays in the unconditioned group were then electrically stimulated during the 72 h PC-12 cell culture. This new group is called Active-Unconditioned, where the term active indicates that the stimulation was delivered during the PC-12 cell culture, as opposed to during the conditioning phase. As summarised in figure 3(a), a total of 5 groups were thus exposed to the PC-12 cell culture and subsequent analysis, as described in section 2.4.2. A total of 3 groups were imaged for protein auto-fluorescence: Stimulated-Conditioned-FCS, Stimulated-Short-Conditioned-HS and Stimulated-Short-Conditioned-SFCM (section 2.5.1, figure 3(b)). Finally, a total of 4 groups were tested with the bicinchoninic acid assay: Stimulated-Short-Conditioned-FCS, Short-Conditioned-FCS, Stimulated-Short-Conditioned-PBS and Short-Conditioned-PBS (section 2.5.2, figure 3(b)).

2.3. Electrode array characterisation

The following techniques were used to characterise the properties of the arrays. Figure 3 shows which method was used for each group of arrays.

2.3.1. Surface topography. The surface profile of the electrode arrays was characterized with vertical scanning interferometry (VSI, ContourGT, Bruker) and scanning electron microscopy (SEM, JEOL JSM 5500 LV). Prior to SEM of cell or protein coated arrays, the arrays were fixed in 2.5% glutaraldehyde in 0.1 M sodium cacodylate buffer for 30 min, and dehydrated in an ascending ethanol series.

2.3.2. Electrical impedance spectroscopy (EIS). Electrode arrays were placed in plastic wells filled with PBS, which served as a conductive electrolyte solution. Using an impedance analyser (6500B series, Wayne Kerr Electronics), the impedance was measured by applying 50 mV sinusoids from 20 Hz to 100 kHz between central and guard electrodes.

2.3.3. Cyclic voltammetry (CV). To measure the electrode charge storage capacity (CSC), electrode arrays were placed in PBS purged with N_2 . Following 30 min settling time, cyclic

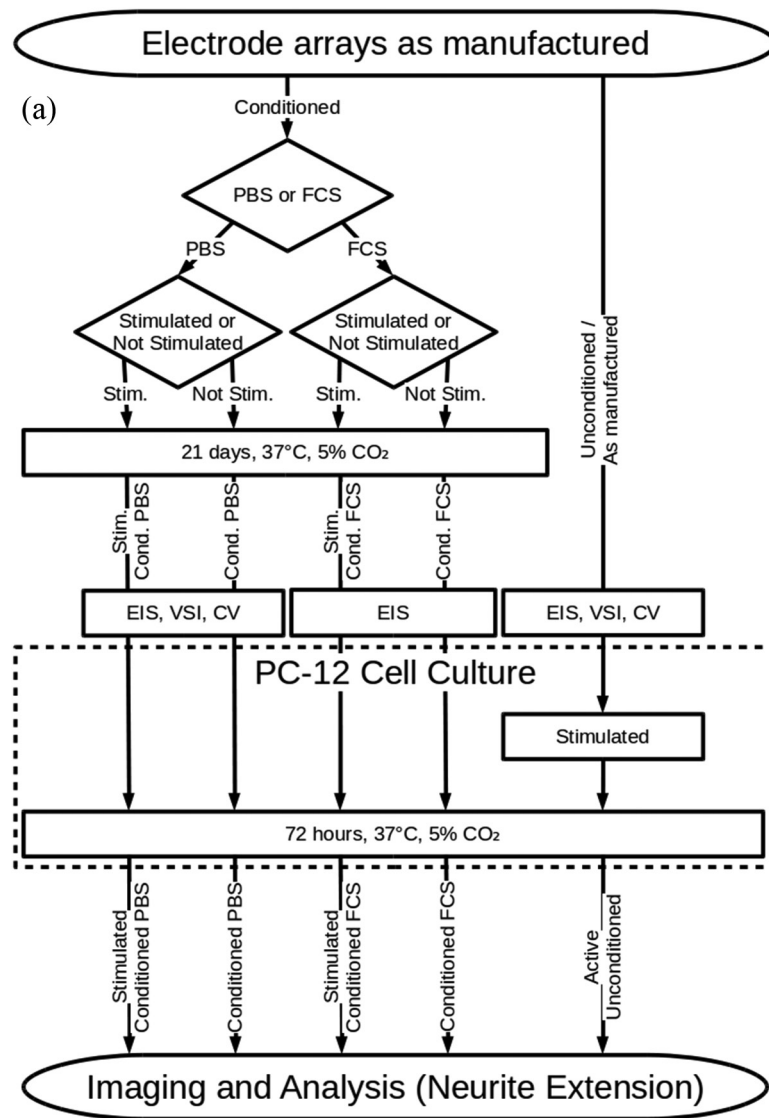


Figure 3. (a) Flowchart of experimental protocol for electrode array conditioning, including stimulation, for PC-12 cell culture and analysis. PBS = phosphate buffered saline, FCS = foetal calf serum, EIS = electrical impedance spectroscopy, VSI = vertical scanning interferometry, CV = cyclic voltammetry.

voltammetry (CV) sweeps were performed using a ModulabXM Potentiostat (Solartron Analytical, USA), with a sweep rate of 50 mV s^{-1} from -0.6 V to $+0.8 \text{ V}$, the water window (Cogan 2008, Green et al 2013). A saturated calomel (SCE) reference electrode and a platinum counter electrode were used, the thick film electrode formed the working electrode (Kumasa et al 2016). Data was recorded using ModulabXM ECS software (version 2.2.x, Solartron Analytical) and analysed using MATLAB (R2013a and R2014b, The MathWorks, Inc.).

2.3.4. Charge injection capacity (Q_{inj}). To determine the charge injection capacity (Q_{inj}) electrode arrays were placed in PBS. Charge controlled biphasic waveforms were applied at 1 kHz through the central electrode using an Ag/AgCl reference electrode and a platinum counter electrode. The maximum negative potential excursion (E_{mc}) and maximum positive potential excursion (E_{ma}) were determined from the voltage transient waveform which was measured differentially

versus Ag/AgCl (see supplementary figure 1 (stacks.iop.org/JNE/14/036012/mmedia), Cogan 2008). The charge injection limit was defined as the charge applied which polarises the electrode to either limit of the water window, -0.6 V (E_{mc}) to $+0.8 \text{ V}$ (E_{ma}). Data was recorded using a digital oscilloscope and analysed using MATLAB (R2013a and R2014b, The MathWorks, Inc.).

2.4. Biocompatibility

2.4.1. Extract assay. Extract tests were performed using the L929 (85011425, Sigma) fibroblastic cell line, following ISO 10993-5 (2009). As illustrated in figure 3(c), electrode arrays at different steps of manufacture (alumina plates with sintered Pt/Au and/or dielectric tracks, and the naked alumina plates) were autoclave sterilized and incubated in PBS at $70 \text{ }^\circ\text{C}$ for 24 h to produce the extracts. 1 ml of extract was produced for every 6 cm^2 of exposed surface (ISO 10993-12 2012).

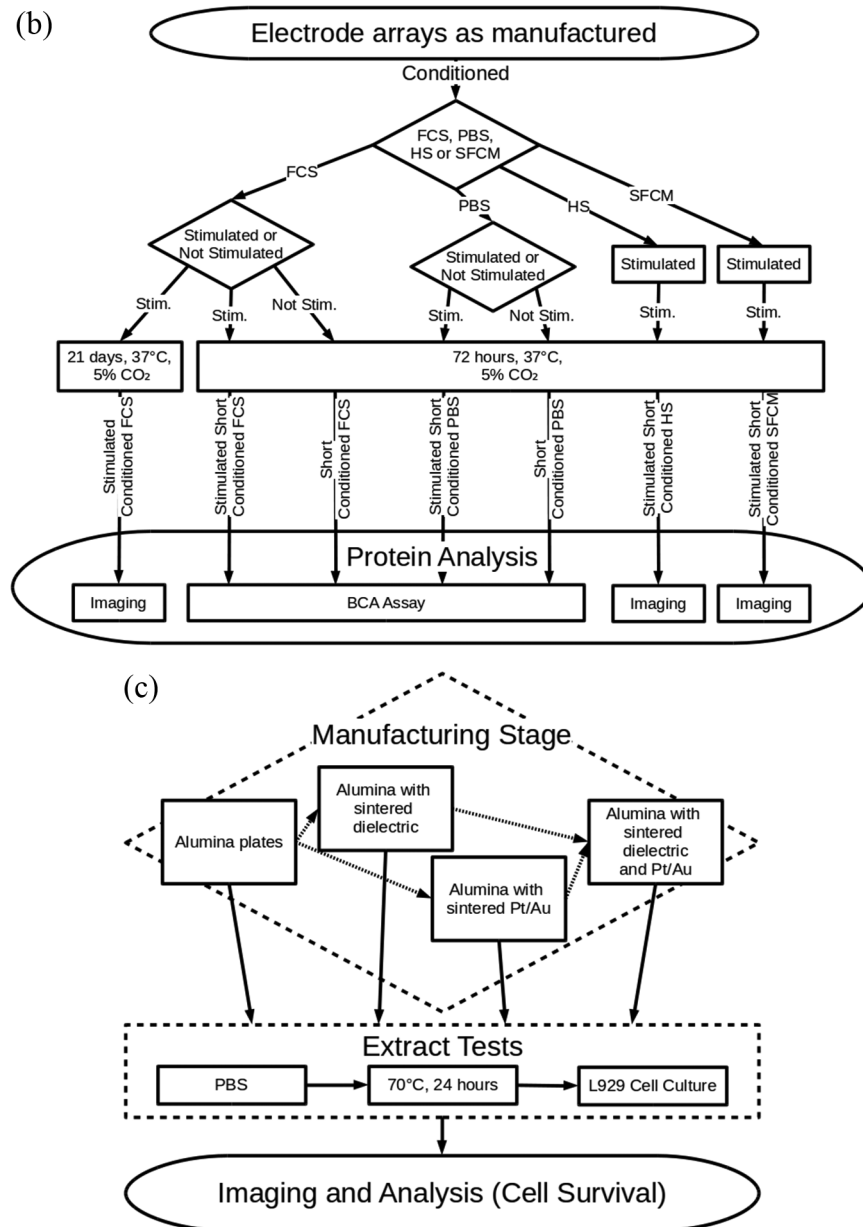


Figure 3. (b) Flowchart of experimental protocol for protein autofluorescence imaging, BCA assay and analysis. FCS = foetal calf serum, PBS = phosphate buffered saline, HS = Horse Serum, SFCM = serum-free culture medium, BCA = bicinchoninic acid. (c) Flowchart of experimental protocol for L929 cells extract test. PBS = phosphate buffered saline, Pt/Au = platinum/gold alloy.

L929 cells (passage 15) were seeded onto 24-well and 96-well cell culture plates, at a density of 20000 cells cm⁻². The culture medium used was high-glucose Dulbecco's modified Eagle's medium (D-6429, Sigma) supplemented with 10% (v/v) foetal calf serum (First Link Ltd.), 100 IU ml⁻¹ penicillin, and 100 µg ml⁻¹ streptomycin (both from Life Technologies). Cells were incubated for 24 h (37 °C, 5% CO₂), to form a semi-confluent monolayer. Medium was replaced with a 25% extract + 75% culture medium solution. Negative controls consisting of high-density polyethylene extracts (HDPE, PUR-1050 Medical Grade UHMWPE, Orthoplastics), positive controls (gradients of phenol or ethanol) and blank controls (PBS) were also used. Cells were exposed to extract solutions or controls for 48 h.

To assess cell survival, cells in 24-well plates were detached from the wells by incubating in trypsin/EDTA (ethylenediaminetetraacetic acid, Life Technologies) at 37 °C, 5% CO₂, for 5 min. A trypan blue viability assay (Sigma) and manual cell counts were performed using a hemocytometer. Metabolic activity assays were carried out on cells in 96-well plates. Extract solutions were replaced with phenol-free culture medium supplemented with 10 µl of MTT (3-(4,5-dimethylthiazol-2-yl)-2,5-diphenyltetrazolium bromide dye, Millipore), and incubated for 4 h at 37 °C. Fluorescent emission was read at 510 nm (Fluoroskan Ascent, ThermoScientific). Measurements were normalized with respect to cells exposed to blank controls.

2.4.2. Neuronal contact assay. The cells of the PC-12 cell line reversibly differentiate into sympathetic-neuron-like cells in the presence of nerve growth factor (NGF), extending neurites and developing electrical excitability (Fujita *et al* 1989). The electrode arrays presented in this study are designed to be in direct contact with neuronal tissue; therefore PC-12 cells were chosen for a contact biocompatibility assay. Cell body density and neurite extension at the electrode sites were used as indicators of biocompatibility. Array treatment conditions for PC-12 cell culture are summarized in figure 3(a).

PC-12 cells (88022401, ECACC) at passage 8 were cultured on poly-D-lysine plated flasks for 7 d in preparation for this assay. RPMI-1640 (Sigma) supplemented with 10 mM HEPES buffer, 1 mM sodium pyruvate, 1% horse serum (all three from Sigma), 50 ng ml⁻¹ NGF, 100 IU ml⁻¹ penicillin, and 100 μg ml⁻¹ streptomycin was used as culture medium. Cells were resuspended in medium containing 100 ng ml⁻¹ NGF, and seeded onto electrode arrays coated with collagen IV (10 μg cm⁻², Sigma), at a density of 20 000 cells cm⁻². Cells were allowed to adhere for 24 h (37 °C, 5% CO₂), before wells were flooded with medium. Cells were incubated for a further 72 h before analysis. During 72 h culture, some of the electrode arrays were stimulated as described in section 2.2, resulting in the group termed Active-Unconditioned, see figure 3(a).

Cells adhered to the arrays were fixed with buffered formalin and stained with FITC conjugated phalloidin (1:100 dilution, Sigma) and DAPI (20 μg ml⁻¹, Sigma). Samples were visualized with a fluorescence microscope (Axioskop 2 Plus, Zeiss). Six images from individual electrode sites were taken for every array and used for analysis. Cell counts were performed using Image-J (v1.48, National Institutes of Health, USA). Neurite outgrowth was quantified using the WIS-NeuroMath software tool (Rishal *et al* 2013). Only extensions longer than the average cell body diameter were considered neurites and were included in the statistical analysis. Contrast and brightness were optimized to facilitate viewing of cells and structures in the figures presented.

2.5. Protein analysis—stimulation in physiological environment

2.5.1. Visual observations. To assess the effects of the *in vivo* environment on electrode array properties, arrays were conditioned in FCS as well as PBS. Analysis (after the PC12-cell culture) of the Stimulated-Conditioned-FCS arrays was not possible due to autofluorescent agglomerates at the electrode sites which impeded the visualisation of the cells. Autofluorescence was also observed on the central electrodes of the Active-Unconditioned arrays. We hypothesized that these agglomerates consisted of serum proteins which had adsorbed to the electrode sites, and carried out further investigation, summarised in figure 3(b).

In a first phase, electrode arrays were conditioned, including stimulation, following the protocol described in section 2.2, for 72 h in culture medium either with, or without, 1% horse serum, to replicate the agglomerates observed on the Active-Unconditioned arrays. These were imaged under fluorescence microscopy and SEM.

2.5.2. BCA (bicinchoninic acid) assay. A BCA assay was carried out to determine the total mass of protein in the agglomerates and adsorbed to the array surface. Due to sputter coating for SEM, further analysis could not be carried out on samples from the first phase. Therefore, in a second phase, electrode arrays were conditioned, with and without stimulation, in either PBS or 100% FCS for 72 h. Arrays were washed in PBS to remove loosely bound protein, and adsorbed protein was removed by incubation for 2 h at 37 °C in protein dissolution buffer (125 mM Tris-HCl pH 7.4, 0.5% SDS) with gentle agitation. Proteins were precipitated from the buffer using acetone, re-dissolved in PBS, and mixed in equal volumes with microBCA reagent (23235, Thermo Scientific). Samples were incubated at 37 °C for 2 h and absorbance was read at 562 nm (M200Pro, Tecan). A bovine serum albumin (BSA, Sigma) standard curve was used to calculate protein concentrations.

2.6. Statistical analysis

Statistical analysis and data plotting was carried out using SPSS (IBM SPSS software, Version 22.0, IBM Corp.). Data from biocompatibility studies were analysed using one-way ANOVA tests (with Bonferroni post hoc comparisons). Where there were non-equal variances (by Levene's tests), data were analysed using Welch's *F*-test followed by Games-Howell post hoc tests rather than Bonferroni post hoc tests. Assumptions of normality were tested using the Shapiro–Wilk test. Paired samples (CV before and after conditioning) were analysed using Wilcoxon Signed-Rank tests due to non-normal distributions. Differences were considered significant when $p < 0.05$. Sample sizes ($n = 5$, $n = 10$) was chosen *a priori*. Data is presented as Tukey boxplots. Values are presented as means ± standard deviation to three significant figures.

3. Results

3.1. Electrode characterisation

3.1.1. Surface topography. VSI on Unconditioned (as manufactured) arrays showed that electrode sites have a diameter of 150 μm, with conductive tracks 90 μm wide. The conductive Pt/Au tracks have a maximum thickness of 15 μm, and the dielectric insulator layer is 10 μm thick (figure 4). Assuming a half-ellipsoid electrode geometry and accounting for adjacent track area not covered by dielectric, Pt/Au electrodes have a geometric surface area of approximately 0.0295 mm². The as manufactured electrodes are rough and highly porous with S_a circa 0.95 μm and surface index circa 3.34 (see table 1). This can also be observed in the scanning electron micrographs (figure 5).

Following 21 d of stimulation in PBS, the electrode surface roughness and surface index increased to $S_a = 1.350 ± 0.400$ μm ($p = 0.010$), and $5.335 ± 1.079$ ($p < 0.001$) respectively. Incubation in PBS without stimulation also increased the surface index significantly, to $4.519 ± 0.754$ ($p = 0.009$), but did not significantly alter the surface roughness ($S_a = 1.058 ± 0.181$ μm, $p = 0.057$). The differences

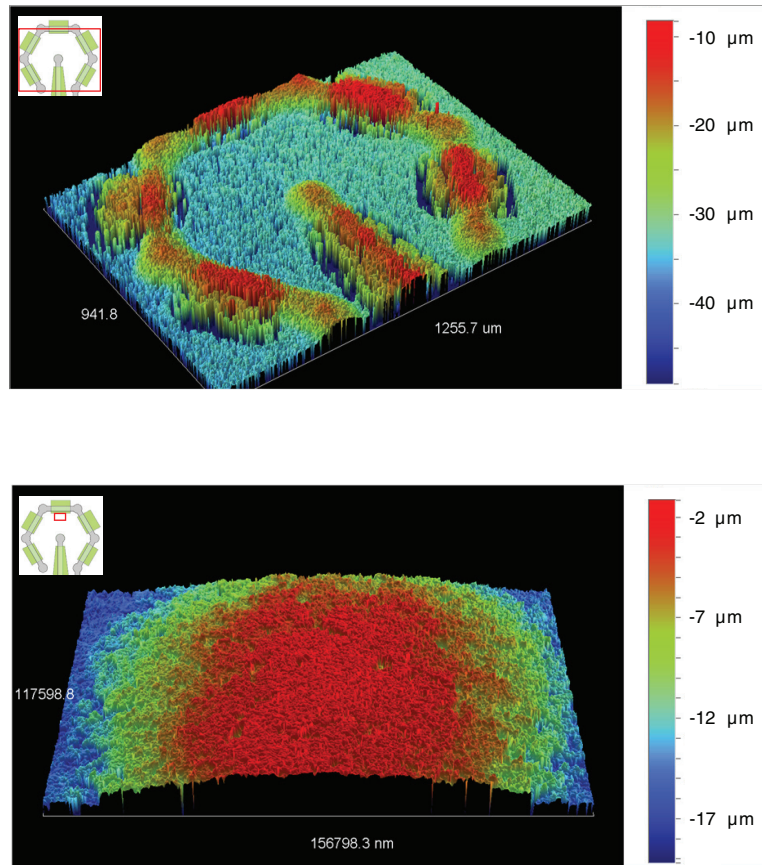


Figure 4. 3D reconstructions of the surface of a hex electrode array (top) and a single electrode site (bottom) produced by vertical scanning interferometry.

Table 1. Surface topography of platinum/gold electrodes printed on alumina (mean \pm S.D. for $n = 10$).

	Before conditioning		After 21 d conditioning	
	Stimulated-conditioned-PBS	Conditioned-PBS	Stimulated-conditioned-PBS	Conditioned-PBS
S^a (μm)	0.952 ± 0.085^a	0.945 ± 0.051	1.35 ± 0.40^a	1.06 ± 0.18
Surface index	3.34 ± 0.24^b	3.48 ± 0.37^c	5.33 ± 1.08^b	4.52 ± 0.75^c

Note: significant differences by paired t -tests are indicated by superscripts.

^a $p = 0.010$, ^b $p < 0.001$, ^c $p = 0.009$.

following stimulation in PBS observed under VSI were not obvious under SEM (figure 5).

3.1.2. Electrical impedance spectroscopy (EIS). EIS was used to characterize the impedance of the electrode arrays. The results are displayed as Bode plots for the Unconditioned, Stimulated-Conditioned-PBS and Stimulated-Conditioned-FCS arrays in figure 6. The results at low (20 Hz), medium (1 kHz) and high (100 Khz) frequencies were compared (table 2).

As described in section 2, the electrode array stability was assessed using biphasic pulses to simulate long-term use (1.8×10^9 pulses throughout a period of 21 d). This corresponds to a cathodic charge density of circa 0.3 mC cm^{-2} w.r.t. geometric area, or 0.09 mC cm^{-2} w.r.t. real area using a

ratio of geometric to real area of 3.48, as calculated from the VSI results (section 3.1).

At low frequency, there were no significant differences between the arrays tested (Welch's F -Test, $p = 0.091$, $F(4, 7.277) = 3.052$). Conditioned-PBS arrays have similar impedance to as manufactured arrays ($p \geq 0.498$). Stimulated-Conditioned-PBS arrays show a decrease in impedance at 1 kHz compared with Unconditioned arrays ($p = 0.044$), with no significant differences at 20 Hz or 100 kHz ($p \geq 0.19$). SEM did not highlight any noticeable differences in topography between these arrays (figure 5), however differences were observed in surface roughness and index (table 1). At 1 kHz, there is significant increase in impedance when arrays are conditioned with serum, with and without stimulation,

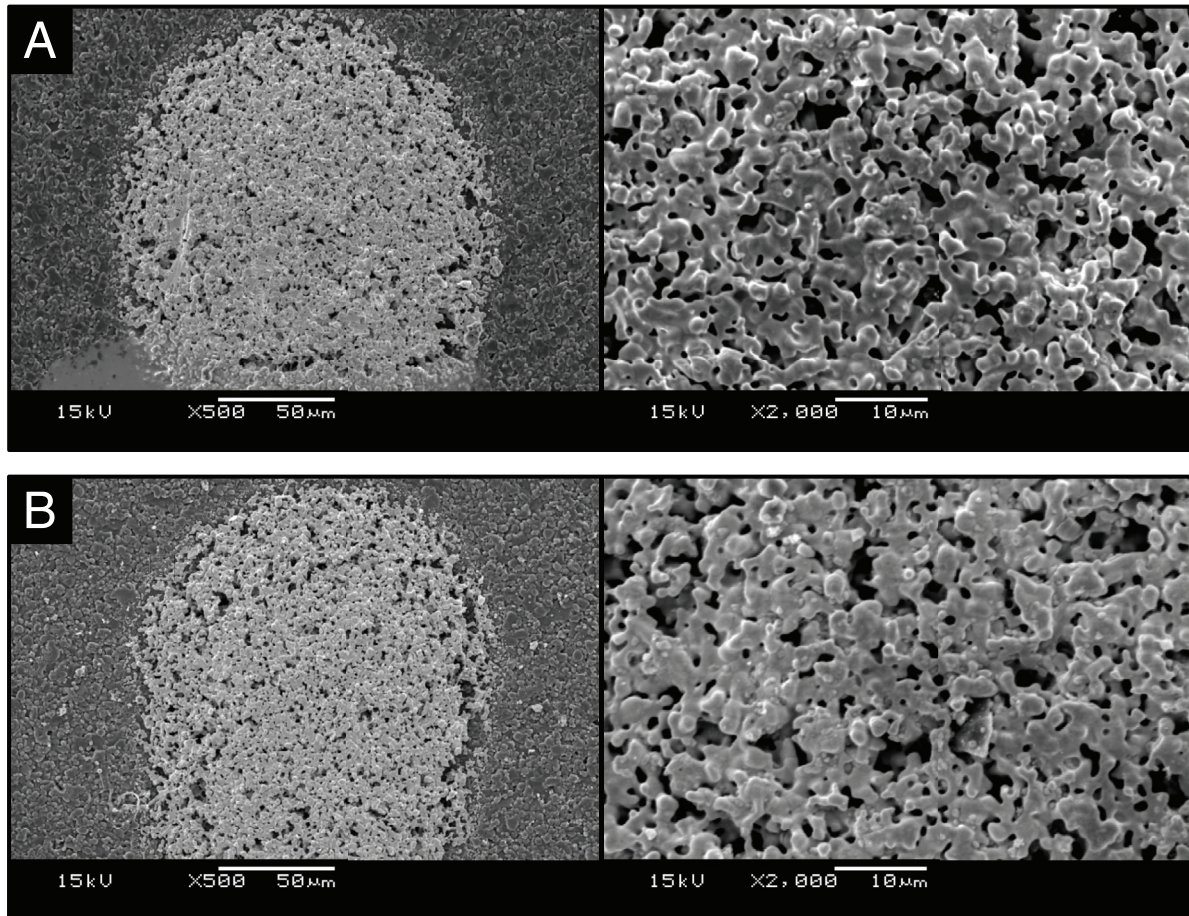


Figure 5. Scanning electron micrographs of an electrode site: (A) as manufactured (Unconditioned); and (B) following delivery of electrical pulses in PBS at 37 °C for 21 d (Stimulated-Conditioned-PBS). On the right, high magnification images of the electrodes ($\times 2000$) make the high porosity of the electrode surface appreciable.

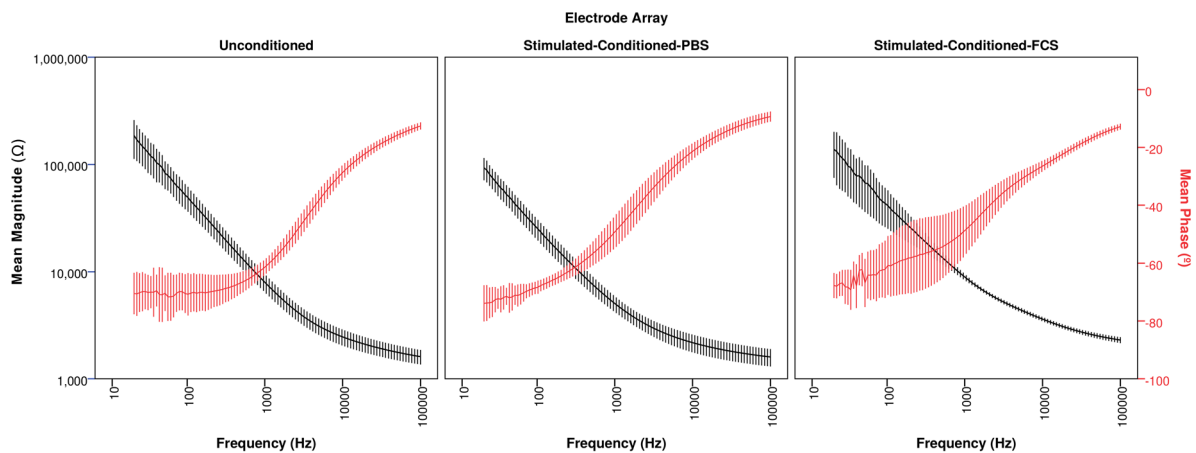


Figure 6. Bode plots of frequency-dependent impedance of electrode arrays as-manufactured (Unconditioned), and following the delivery of electrical stimuli for 21 d in either PBS (Stimulated-Conditioned-PBS) or foetal calf serum (Stimulated-Conditioned-FCS). Data presented as mean \pm SD, for $n = 5$ electrode arrays.

compared with conditioning in PBS ($p \leq 0.004$). At 100 kHz, this increase is only observed for arrays stimulated in serum compared with PBS ($p = 0.012$).

3.1.3. Cyclic voltammetry (CV). CV responses to a 50 mV s^{-1} sweep were measured with either the central cathode or ring electrodes as working electrode. CV response normalized to

electrode geometric area is shown in supplementary figures 2 and 3. CSCs and cathodic CSCs (cCSC) for Unconditioned, Conditioned-PBS and Stimulated-Conditioned-PBS arrays are reported in table 3.

Prior to conditioning in PBS cCSC of central electrodes were significantly different while all other values were not significantly different. Stimulation in PBS increases CSC and

Table 2. Impedance (|Z|) of thick-film platinum/gold electrodes printed on alumina (mean \pm S.D. for $n = 5$).

Frequency	Impedance (Z , in k Ω)				
	Unconditioned	Stimulated-conditioned-PBS	Conditioned-PBS	Stimulated-conditioned-FCS	Conditioned-FCS
20 Hz	187 \pm 74	93.2 \pm 9.8	126 \pm 28	139 \pm 28	285 \pm 80
1 kHz	7.73 \pm 1.49 ^a	4.93 \pm 0.83 ^{a,b}	6.46 \pm 1.68 ^c	8.72 \pm 0.57 ^b	10.8 \pm 2.1 ^c
100 kHz	1.61 \pm 0.25 ^d	1.60 \pm 0.30 ^e	1.78 \pm 0.40	2.30 \pm 0.15 ^{d,e}	1.76 \pm 0.30

Note: significant differences by Bonferroni post hoc tests are indicated by superscripts.

^a $p = 0.044$, ^b $p = 0.003$, ^c $p = 0.004$, ^d $p = 0.014$, ^e $p = 0.012$.

Table 3. Charge storage capacities (CSC) and cathodic CSCs (cCSC) of thick-film platinum/gold electrodes printed on alumina, normalized to geometric area (mean \pm S.D. for $n = 10$).

	Central electrode			
	Before conditioning (unconditioned)		After 21 d conditioning	
	Stimulated-conditioned-PBS	Conditioned-PBS	Stimulated-conditioned-PBS	Conditioned-PBS
CSC (mC cm ⁻²)	9.41 \pm 3.52 ^a	7.05 \pm 1.78	16.1 \pm 7.0 ^{a,b}	9.89 \pm 4.50 ^b
cCSC (mC cm ⁻²)	5.51 \pm 2.08 ^{c,d}	8.41 \pm 2.84 ^c	5.56 \pm 1.15 ^{d,e}	5.19 \pm 0.86 ^e
	Ring electrodes			
	Before conditioning (unconditioned)		After 21 d conditioning	
	Stimulated-conditioned-PBS	Conditioned-PBS	Stimulated-conditioned-PBS	Conditioned-PBS
CSC (mC cm ⁻²)	10.8 \pm 3.1	9.16 \pm 2.23 ^f	9.60 \pm 1.80 ^g	7.56 \pm 0.94 ^{f,g}
cCSC (mC cm ⁻²)	4.07 \pm 0.95	4.98 \pm 1.13 ^h	5.21 \pm 2.50 ⁱ	4.15 \pm 0.40 ^{h,i}

Note: significant differences by Wilcoxon Signed-Rank tests are indicated by superscripts.

^a $p = 0.012$, ^b $p = 0.002$, ^c $p = 0.036$, ^d $p = 0.048$, ^e $p < 0.001$, ^f $p = 0.024$, ^g $p < 0.001$, ^h $p = 0.024$, ⁱ $p < 0.001$.

cCSC: for ring and central electrodes compared with electrodes which had not undergone stimulation ($p \leq 0.002$); and for central electrodes compared with the same electrodes prior to stimulation ($p \leq 0.048$).

3.1.4. Charge injection capacity (Q_{inj}). Electrode Q_{inj} increased following 21 d in PBS, with and without stimulation (see table 4). There was no significant difference in Q_{inj} after 21 d conditioning compared with before conditioning for stimulated electrodes $t(4) = -1.918$, $p = 0.128$, and not-stimulated electrodes $t(4) = -3.097$, $p = 0.036$, $\alpha_{bonferroni} = 0.025$. There was no significant difference in Q_{inj} after 21 d conditioning between Stimulated-Conditioned-PBS samples and Conditioned-PBS samples, $t(4) = 0.262$, $p = 0.806$. A Shannon Plot (log-D versus log-Q) of Q_{inj} before and after conditioning is given in supplementary figure 4 with charge density normalised to real and geometric areas (Shannon 1992, Cogan et al 2016).

3.2. Biocompatibility

3.2.1. Extract assay. To evaluate electrode array cytotoxicity, extract tests were performed using the L929 fibroblast cell line, as illustrated in figure 3(c). Of the samples tested (alumina ceramic plates, alumina with sintered Pt/Au tracks, alumina with sintered dielectric, and final construct), none of the leachants were found to have a significant effect on cell survival (trypan blue assay, $p = 0.336$) or metabolic activity

(MTT assay) ($p = 0.054$, $n = 5$) compared with HDPE extract negative controls (figure 7 and supplementary figure 5).

3.2.2. Neuronal contact assay. Contact biocompatibility assays were performed with PC-12 cells cultured on Conditioned-PBS, Stimulated-Conditioned-PBS, Conditioned-FCS, Stimulated-Conditioned-FCS, and Active-Unconditioned electrode arrays (figure 3(a)). Intense protein autofluorescence prevented analysis of the Stimulated-Conditioned-FCS electrode arrays. The results reported hereafter therefore only concern the Conditioned-PBS, Stimulated-Conditioned-PBS, Conditioned-FCS, and Active-Unconditioned electrode arrays.

PC-12 cells were significantly increased in number at the electrode sites relative to controls cultured on collagen-coated glass coverslips ($p < 0.001$, $n = 5$). PC-12 cells extended neurites in all electrode array treatment conditions tested. Cells tended to extend more neurites when grown on arrays compared with controls, with cells in the Active-Unconditioned and Conditioned-FCS groups expressing significantly more neurites ($p = 0.013$ and $p = 0.043$, respectively, $n = 5$). These results are shown in figure 8. Neurite length on arrays was not significantly different to coverslip controls. Controls demonstrated that the addition of NGF did not affect PC-12 cell density, and that without NGF PC-12 cells did not express neurites.

Table 4. Charge injection capacity (Q_{inj}) per cathodic phase of thick-film platinum/gold electrodes printed on alumina normalized to geometric area and real area (mean \pm S.D. for $n = 5$).

	Before conditioning		After 21 d conditioning	
	Unconditioned	Stimulated-conditioned-PBS	Conditioned-PBS	
Q_{inj} (mC cm ⁻²) w.r.t. Geometric Area	0.373 \pm 0.244 ^{a,b}	0.748 \pm 0.150 ^{a,c}	0.722 \pm 0.226 ^{b,c}	
Q_{inj} (mC cm ⁻²) w.r.t. Real Area	0.115 \pm 0.075	0.136 \pm 0.025	0.148 \pm 0.052	

Note: no significant differences were observed, results of paired two sample *t*-tests are indicated by superscripts.

^a $t(4) = -1.918, p = 0.128$, ^b $t(4) = -3.097, p = 0.036$, $\alpha_{\text{bonferroni}} = 0.025$, ^c $t(4) = 0.262, p = 0.806$.

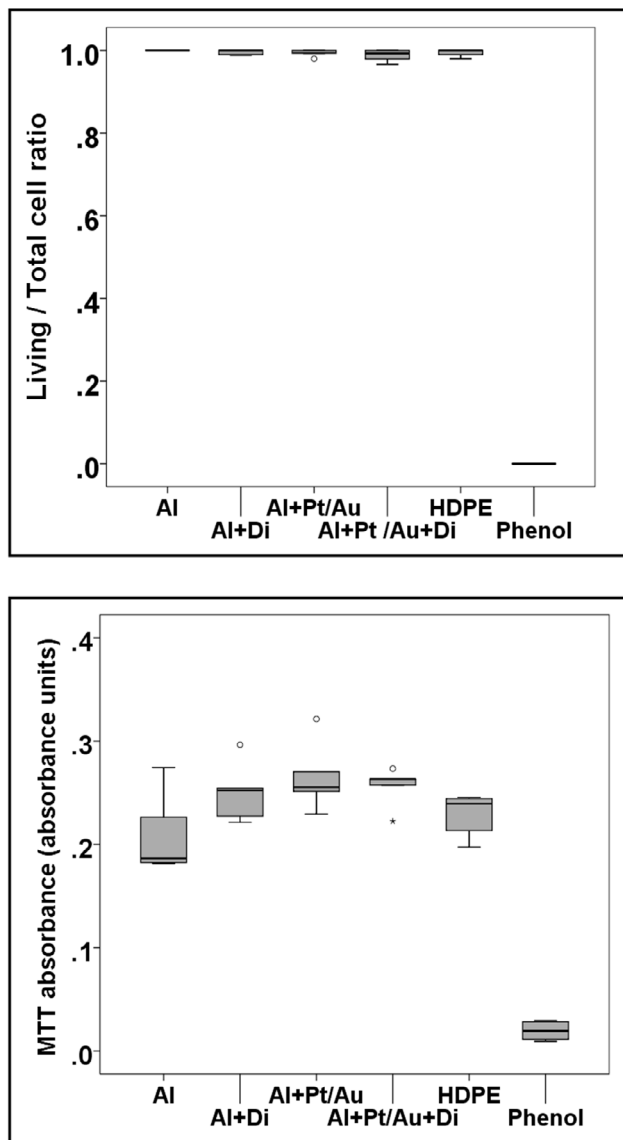


Figure 7. Effect of sample extracts on L929 fibroblast cell line. (Top) Quantification of cell survival (fraction of cells alive) as determined by trypan blue viability assay. (Bottom) Quantification of MTT assay for cell metabolic activity. Data represented as box plots for $n = 5$ cell wells. Al = alumina; Di = sintered dielectric; Pt/Au = sintered platinum/gold; HDPE = high density polyethylene negative control; phenol = phenol positive control.

Although we did not quantify this, PC-12 cell attachment to the dielectric surface was poor. This may be due to the material physical properties and not due to cytotoxicity. Growth of cells in the vicinity of the dielectric was not impaired, and extract tests show no impact of this material on L929 cell metabolic activity or survival (results presented in section 3.2.1).

3.3. Protein analysis—stimulation in physiological environment

3.3.1. Visual observations. Figure 9 shows fluorescence microscopy and SEM images of electrode arrays: stimulated for 21 d in 100% foetal calf serum (left column); stimulated for 3 d in culture medium containing 1% horse serum (middle column) and stimulated for 3 d in serum free culture medium. The autofluorescent agglomerates are visible on the anodes and cathode after 21 d in 100% FCS (Stimulated-Conditioned-FCS) as well as on the central cathode after 3 d of stimulation in culture medium containing 1% horse serum, but not on the ring electrodes stimulated for 3 d in the 1% horse serum medium, nor on any electrodes stimulated in the serum free medium. Agglomerates were also absent from Conditioned-FCS arrays.

3.3.2. BCA assay. A set of arrays as-manufactured were conditioned, with and without stimulation, for 3 d (figure 3(b)) in either FCS or PBS. BCA assays determined that the Short-Conditioned-FCS arrays had a larger mass of protein than their stimulated counterparts: 199.71 ± 89.05 and 81.12 ± 63.85 μg of protein, respectively ($p = 0.018, n = 3$). Stimulated-Conditioned-PBS arrays contained considerably less protein, at 4.91 ± 2.1 μg ($n = 3$). Measurements from Conditioned-PBS arrays were below the detection level of the assay (i.e. < 1 μg in this experiment, $n = 3$).

4. Discussion

4.1. Electrode characterisation

Thick-film printing techniques can be used to produce electrode arrays at densities of hundreds of electrode sites per cm², with each individual electrode being ≥ 50 μm in diameter. Electrode arrays of similar dimensions to those tested here

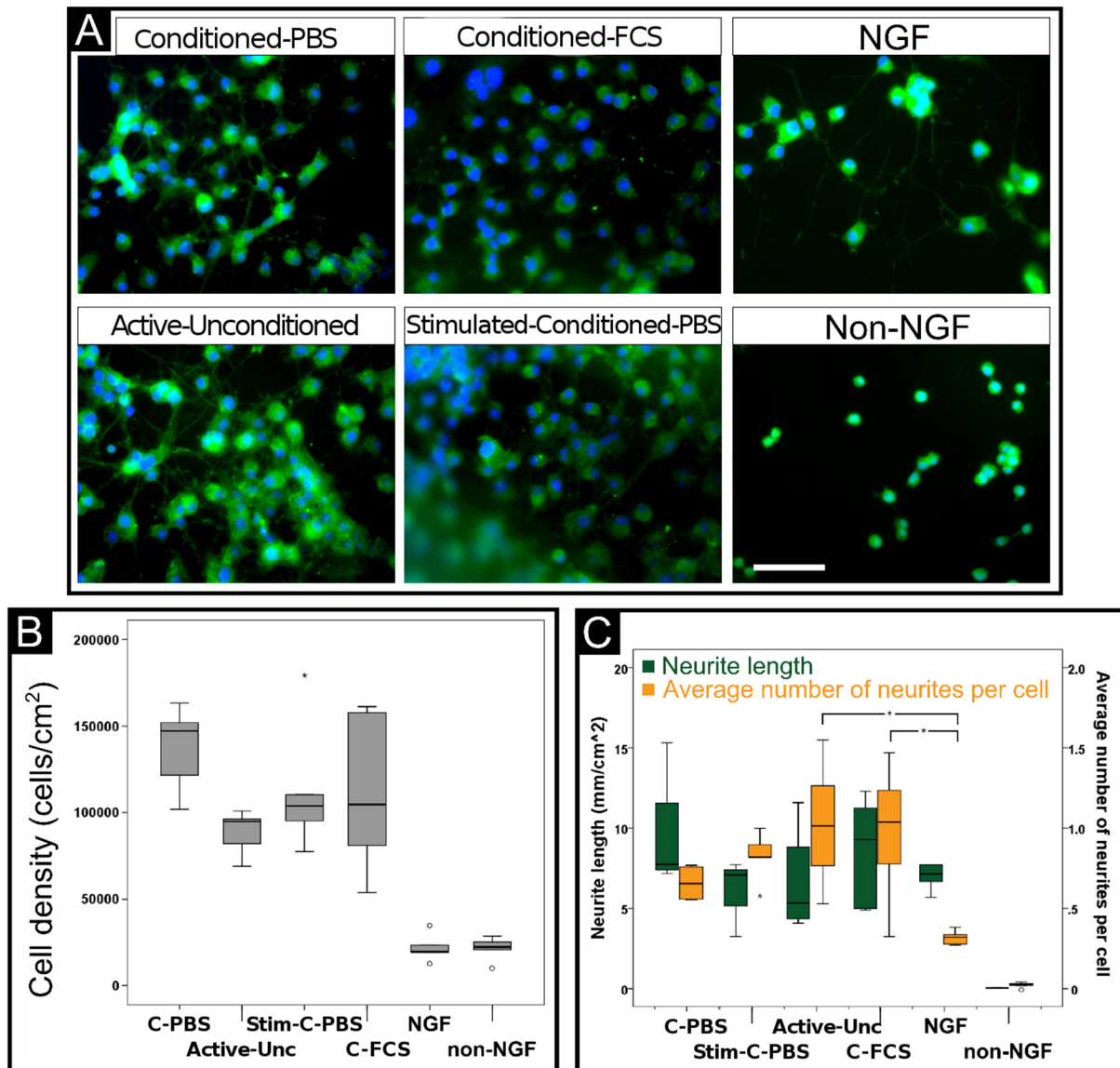


Figure 8. Survival and differentiation of PC-12 cells on electrode arrays. (A) Representative images of cell nuclei (blue) and actin filaments (green) following culture of cells on electrode surface for 96h. Scale bar: 50 μm . (B) Quantification of PC-12 cell density on the electrode sites. (C) Quantification of measured neurite longitude (green) and average number of neurites per cell (orange). For all shown experiments, $n = 5$ pairs of hexagonal electrode arrays. C-PBS = Conditioned-PBS, Active-Unc = Active-Unconditioned, Stim-C-PBS = Stimulated-Conditioned-PBS, C-FCS = Conditioned-FCS, NGF = control containing nerve growth factor on glass cover slips, non-NGF = control without nerve growth factor on glass cover slips.

(150 μm in diameter) but micromachined out of Pt foil embedded in PDMS (polydimethylsiloxane), have been used to stimulate retinal tissue (Suaning *et al* 2007, Dodds *et al* 2009). Our thick-film electrodes remain functional following 21 d of continuous stimulation with electrical pulses comparable to those used *in vitro* and *in vivo* (Sachs *et al* 2004, Wong *et al* 2009, Zeng *et al* 2009, Green *et al* 2014). The Pt/Au thick-film ink produces very porous structures, which results in low electrode impedance and high cell adherence. Electrode arrays and their component materials are found to be biocompatible *in vitro* and support stimulation of neuronal-like cells.

Thick-film printing can produce features as small as 50 μm . This accuracy can be used to screen print electrodes with a

pitch as low as 150 μm . Smaller feature sizes are limited by screen production and inaccuracies introduced by the flow of the thick-film inks. This may be overcome by defining the array pattern with a laser post-printing, which has been shown to lower the pitch to 75 μm (Ordóñez *et al* 2009). The need for conductive tracks limits electrode densities, we estimate thick-film printing will produce functional arrays with 20–25 electrodes mm^{-2} . Despite the simplicity of the printing technique, this approaches density values of state-of-the-art electrode arrays. Platinum arrays on high-temperature co-fired ceramic (HTCC), for example, can be manufactured at 49 electrodes mm^{-2} (unpublished work). For comparison, laser-cut Pt foil electrodes encapsulated in PDMS have achieved 0.33 electrodes mm^{-2} (Henle *et al* 2009), while recent electrode array

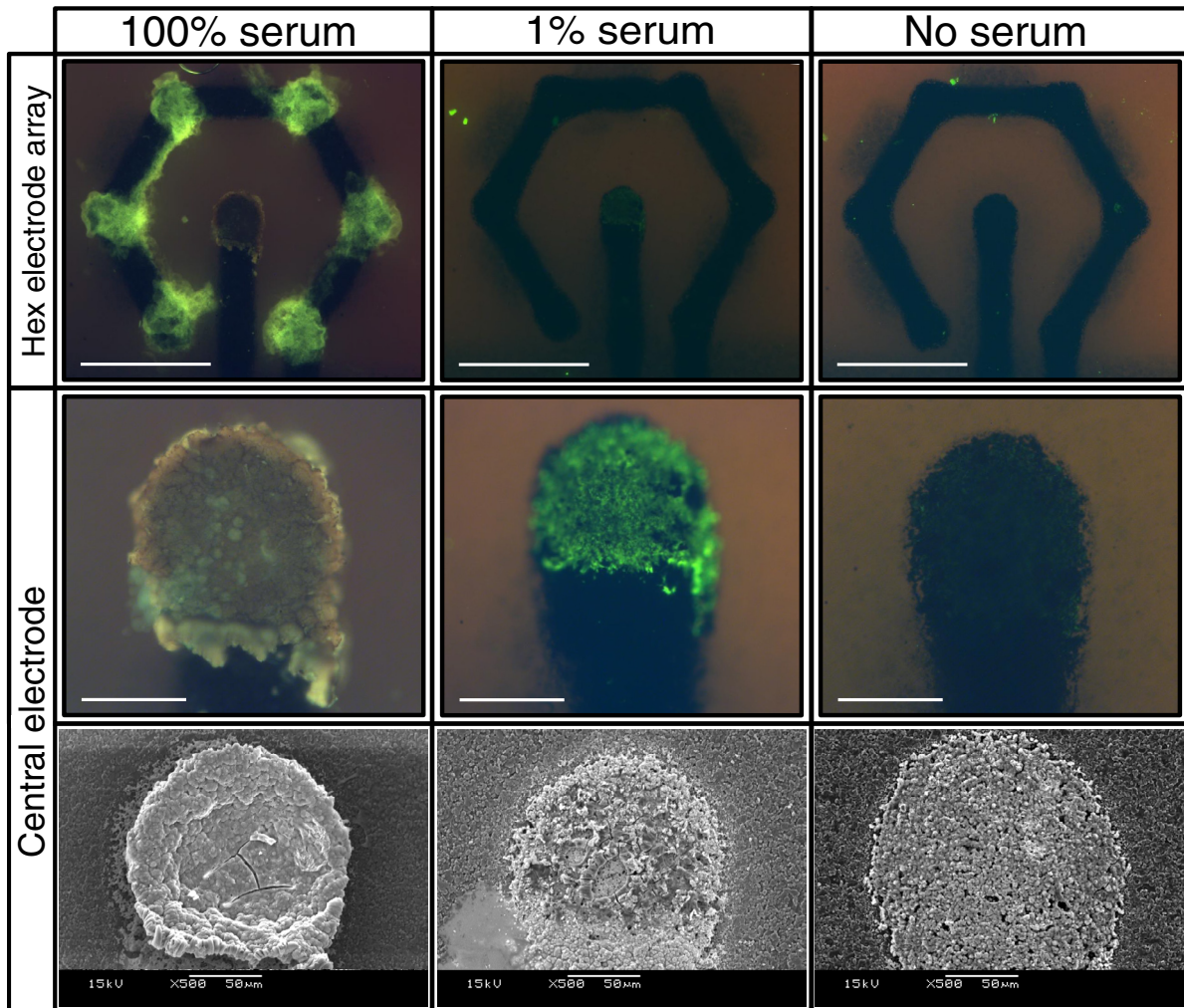


Figure 9. Electrodes following electrical stimulation in different media, visualized under a fluorescence (top and middle rows) and scanning electron microscope (bottom row). Protein adsorption can be seen to occur on the electrodes exposed to pure serum for 21 d (left column) and to a lesser extent on electrodes exposed to 1% serum in culture medium for 3 d (middle column), but not on electrodes stimulated in culture medium with no serum for 3 d (right column). Green: protein agglomerates (autofluorescence), red: alumina (autofluorescence). Scale bars: 500 μm (top row), 100 μm (middle row), and 50 μm (bottom row).

designs using photolithographic, thin-film and CMOS fabrication processes have achieved densities >200 electrodes mm^{-2} (Gunning *et al* 2013, Khodagholy *et al* 2015, Rios *et al* 2016).

We chose to arrange our electrodes in hexagonal units. This hex electrode arrangement has been observed to limit undesired spread of current (Abramian *et al* 2011), and has been previously used *in vitro* (Green *et al* 2013). Parameters such as electrode density, feature size, and geometric distribution are readily changed by modifying the screens used for printing. Users will modify these parameters to tailor the thick-film arrays to their specific application. Moreover, although we limited our design to a single layer of conductor covered by a single layer of dielectric, this can be expanded. Multiple layers of conductor/insulator may be stacked to allow more complex overlapping circuit arrangements, requiring no additional materials or equipment beyond that presented in this work. This approach may also be used to build 3D features. Our two printed layers have a combined thickness of 25 μm , and further layers could be added to increase the height of

the electrodes. Using this method, we have produced dome shaped electrodes protruding by an additional 25 μm over the dielectric (unpublished work).

The electrodes produced by thick-film printing have unusual surface properties. Thick-film inks consist of metal or ceramic particles suspended in an organic vehicle. During drying and sintering the vehicle evaporates, and the particles coalesce into a highly porous material (Nam *et al* 2006). This porosity can be appreciated in SEM and VSI images of the electrode surface (figures 4 and 5), and was quantified to translate to a circa $3.4 \times$ greater real surface area compared with geometric surface area, although this may be an underestimate due to the line-of-sight limitations of VSI. This compares to surface indexes of 1.7 for compressed Pt particulate (Green *et al* 2013), 1.2 for Pt foil electrodes, increasing to 2.9 with additional surface treatment (Dodds *et al* 2009, Green *et al* 2012a, Green *et al* 2014), and 1.4 for electrodes made by melting Pt wires (Brummer *et al* 1977). Following stimulation and conditioning *in vitro* surface roughness and surface index

increased. After 21 d real surface area was circa $5.3 \times$ greater than geometric surface area. This may indicate loss of electrode material through etching, dissolution, or adhesive failure, although this was not observed under SEM.

Porosity is an important property in electrically active surfaces, determining the surface area over which charge transfer may occur. Higher total surface area equates to lower double-layer capacitance, and a reduction in the electrode's electrical impedance modulus (Franks *et al* 2005). Even small increases in electrode surface may dramatically decrease their electrical impedance (Delivopoulos *et al* 2012). Electrical impedance spectroscopy of our electrode arrays is in line with this concept: thick-film electrodes had generally lower impedance modulus than Pt foil and thin-film smooth Au electrodes of similar dimensions, and similar impedance to other sintered electrodes (Delivopoulos *et al* 2012, Green *et al* 2013, 2014). As manufactured, the arrays have a 1 kHz impedance magnitude of 7.73 ± 1.49 k Ω . Incubation in PBS for 21 d had little effect on the impedance magnitude. These values also appear relatively stable after extensive stimulation (1.8×10^9 electrical pulses over 21 d in PBS, Green *et al* 2012a, 2013), except for a significant decrease in impedance at 1 kHz, in line with the increase in surface area observed by VSI.

CSC, and cCSC, of our arrays as manufactured was comparable to values published for laser-roughened Pt foil arrays of similar geometry (Green *et al* 2012a). The CSC and cCSC increased after 21 d of intensive stimulation in PBS compared to incubation in PBS without stimulation, and may be explained by the increase in available surface (Green *et al* 2014).

Q_{inj} of our thick-film Pt/Au electrodes is similar to that reported by Green *et al* (2013) for sintered Pt electrodes on ceramic (0.21–0.24 mC cm⁻² for pulse widths of 0.2–0.8 ms) and Pt foils roughened by structured laser interference patterning (0.13–0.36 mC cm⁻² for pulse widths of 0.1–0.8 ms, Green *et al* (2014)). These values are higher than those of Pt foil electrodes, which are in the range of 0.05–0.15 mC cm⁻² for similar width pulses (Rose and Robblee 1990, Green *et al* 2012a), but lower than values reported for Pt electrodes coated with conductive polymers (Green *et al* 2012b). The porous nature of sintered Pt, compared to smooth Pt foil, is likely to be responsible for this increase in the injection limit. The increase in Q_{inj} following conditioning in PBS with and without stimulation to >0.7 mC cm⁻² is almost entirely explained by the increase in surface available for charge transfer: the circa $2 \times$ increase in Q_{inj} w.r.t. geometric surface area, is circa $1.2 \times$ when normalised by surface index.

4.2. Biocompatibility

One of the major concerns related to the use of commercial thick-film inks is the presence of additives which may impair cell function—since these inks are not designed for this purpose and their composition is not publicly available. We have shown that the materials used to manufacture the arrays—including the Pt/Au and the dielectric inks—do not reduce cell survival or metabolic activity relative to biocompatible controls. Moreover, we observed that neuronal cell lines cultured

on electrode surfaces preferentially adhere to and extend processes on the porous surface of the electrode sites. Preference for rough surfaces has been previously described in both neuronal and glial cells (Sorkin *et al* 2009). The porosity of the electrodes may therefore be beneficial, enhancing signal detection and stimulation efficiently by integrating with the target cells.

The arrays presented are based on an alumina ceramic plate. Ceramic arrays with sputtered thin-film platinum electrodes have been used as cortical biosensors and recording arrays (Burmeister *et al* 2000, Moxon *et al* 2004, Burmeister *et al* 2005, Miller *et al* 2015). Evaluation of these arrays following implantation showed mild glial scarring and ‘minimal tissue damage’ up to 6 months (Hascup *et al*, 2009). The ceramic substrate also presents a range of possibilities in addition to electrode array manufacture: for example the manufacture of hermetic feedthroughs (Green *et al* 2013, Guenther *et al* 2014), interconnects (Vanhoestenbergh *et al* 2012, Fiedler *et al* 2013), and chip scale bonding (Guenther *et al* 2011).

4.3. Stimulation in physiological environment

Implantable electrode arrays face challenges presented by the *in vivo* biological response. Immediately following implantation, proteins adsorb to the implant surface, forming a layer in a process termed biofouling (Anderson *et al* 2008). Most of these are blood serum proteins, such as albumin and fibrinogen, which spontaneously and non-specifically adsorb to surfaces through non-covalent interactions. The resulting protein layer may impact on the properties of the electrodes, in particular increasing their impedance (Newbold *et al* 2010) and reducing the charge injection limit (Green *et al* 2014). This process is also relevant for arrays intended to be used solely *in vitro*: cell culture media are often supplemented with serum. To simulate the interactions of serum proteins and our electrode arrays, we electrically stimulated arrays in 100% foetal calf serum for 21 d. We report on the formation of large autofluorescent agglomerates (figure 9), presumed to be adsorbed proteins. The autofluorescent agglomerates are visible on the anodes and cathode after 21 d in 100% FCS (Stimulated-Conditioned-FCS) as well as on the central cathode after 3 d in culture medium containing 1% horse serum, but not on any electrodes stimulated in serum free medium. Agglomerates were also absent from Conditioned-FCS arrays. This points to the importance of both the presence of serum, and the stimulation, for their formation. Proteins may be attracted to the electrode surface by charge accumulation due to DC offset, as they are electrically charged (Rugheimer *et al* 2008). Our observations of the arrays stimulated in culture medium with 1% horse serum further indicate that a higher current density promotes agglomerate formation since the agglomerate in this case was only visible on the central cathode, where the current density was $6 \times$ greater than that of the anodes. The stimulation pulses are charge-balanced, hence the current direction is reversed after the stimulating pulse, which prevents any conclusion as to the polarity of the agglomerates. Interestingly, the BCA assay measured a lower amount of protein on the Stimulated-Conditioned-FCS arrays compared to

the Conditioned-FCS arrays, on which the proteins had therefore passively adsorbed. These results conflict, particularly since non-stimulated electrodes did not present any autofluorescent aggregates on visual inspection. This calls for further investigation, such as protein conformation and absorbed layer composition, to determine whether the autofluorescence seen in arrays stimulated in serum is not caused by proteins, or indeed whether this effect is consistent across a large range of electrode arrays.

Despite the presence of these agglomerates on the arrays stimulated in FCS for 21 d, their impedance response was similar to that of the Unconditioned arrays, as seen in the Bode plot of the Stimulated-Conditioned-FCS arrays (figure 6). The presence of serum in the environment might be considered to increase the arrays impedance, however, our results are inconclusive, as seen in table 2. The presence of proteins in solution and adsorbed to the surfaces may be protective, inhibiting structural changes and Pt electrode dissolution (Robblee et al 1980, Green et al 2014).

Protein adsorption to implanted materials or cell culture surfaces occurs whenever serum is present in the medium. However, the nature and effect of this coating is largely dependent on the properties of the surface it adsorbs to. Heavier serum proteins—such as fibronectin and vitronectin—tend to adsorb preferentially to hydrophilic surfaces, and enhance cell attachment (Steele et al 1995, Collier et al 1997). Smaller proteins like complement factors or immunoglobulins are instead enriched in hydrophobic surface layers, and may trigger inflammation and implant rejection (Wilson et al 2005, Anderson et al 2008). We find that PC-12 cells cultured on electrode arrays pre-conditioned in serum exhibit a higher degree of neurite extension, which may indicate that the formation of an attachment-promoting protein layer on our electrode arrays has a positive impact on cells. Whether this extends to *in vivo* implantation, however, is not possible to predict with only the available data.

5. Conclusion

We have reported on the *in vitro* properties of a high-density Pt/Au electrode array manufactured using thick-film printing techniques. The arrays have electrical and topological properties comparable to other arrays manufactured using more complex and expensive techniques, and support the growth of neuronal cell lines. These findings, combined with the versatility and facility for mass production of thick-film printing, make it an attractive platform for the low-cost production of customisable electrode arrays with applications in tissue engineering and neuroscience research.

Acknowledgments

The authors wish to acknowledge: Professor Nick Donaldson for use of the UCL Implanted Devices Group cleanroom and equipment; Ms B Vekaria and Mr D McCreary for technical assistance with the microBCA assay; Ms C Walsh for advice

and assistance with MATLAB; and Ms R Porter for technical assistance with *in vitro* cell culture. HL wishes to acknowledge Engineering and Physical Sciences Research Council (UK), for financial support under their Centres for Doctoral Training scheme (grant EP/G036675/1), and under their Doctoral Prize Fellowship scheme.

References

- Abramian M, Lovell N H, Morley J W, Suaning G J and Dokos S 2011 Activation of retinal ganglion cells following epiretinal electrical stimulation with hexagonally arranged bipolar electrodes *J. Neural Eng.* **8** 035004
- Albareda-Sirvent M, Merkoçi A and Alegret S 2000 Configurations used in the design of screen-printed enzymatic biosensors. A review *Sensors Actuators B* **69** 153–63
- Anderson J M, Rodriguez A and Chang D T 2008 Foreign body reaction to biomaterials *Semin. Immunol.* **20** 86–100
- Bilitewski U, Rürger P and Schmid R D 1991 Glucose biosensors based on thick film technology *Biosens. Bioelectron.* **6** 369–73
- Borkholder D A, Bao J, Maluf N I, Perl E R and Kovacs G T A 1997 Microelectrode arrays for stimulation of neural slice preparations *J. Neurosci. Methods* **77** 61–6
- Brummer S B and Turner M J 1977 Electrical stimulation with Pt electrodes: a method for determination of 'real' electrode areas *IEEE Trans. Biomed. Eng.* **24** 436–9
- Burmeister J J, Moxon K and Gerhardt G A 2000 Ceramic-based multisite microelectrodes for electrochemical recordings *Anal. Chem.* **72** 187–92
- Burmeister J J, Palmer M and Gerhardt G A 2005 l-lactate measures in brain tissue with ceramic-based multisite microelectrodes *Biosens. Bioelectron.* **20** 1772–9
- Churchland M M, Yu B M, Sahani M and Shenoy K V 2007 Techniques for extracting single-trial activity patterns from large-scale neural recordings *Curr. Opin. Neurobiol.* **17** 609–18
- Cogan S F 2008 Neural stimulation and recording electrodes *Annu. Rev. Biomed. Eng.* **10** 275–309
- Cogan S F, Ludwig K A, Welle C G and Takmakov P 2016 Tissue damage thresholds during therapeutic electrical stimulation *J. Neural Eng.* **13** 021001
- Collier T O, Jenney C R, DeFife K M and Anderson J M 1997 Protein adsorption on chemically modified surfaces *Biomed. Sci. Instrum.* **33** 178–83
- Collinger J L, Wodlinger B, Downey J E, Wang W, Tyler-Kabara E C, Weber D J, McMorland A J, Velliste M, Boninger M L and Schwartz A B 2013 High-performance neuroprosthetic control by an individual with tetraplegia *Lancet* **381** 557–64
- Delivopoulos E, Chew D J, Minev I R, Fawcett J W and Lacour S P 2012 Concurrent recordings of bladder afferents from multiple nerves using a microfabricated PDMS microchannel electrode array *Lab Chip* **12** 2540–51
- Dodds C W D, Wong Y T, Byrnes-Preston P J, Rendl M, Lovell N H and Suaning G J 2009 Performance of laser fabricated stimulating electrode arrays for a retinal prosthesis in saline *4th Int. IEEE/EMBS Conf. on Neural Engineering, 2009. NER '09* pp 88–91
- Fiedler E, Ordóñez J S and Stieglitz T 2013 Laser-structured ceramic adapters for reliable assembly of flexible thin-film electrodes *Biomed. Eng. Biomed. Tech.* **58** S1
- Franks W, Schenker I, Schmutz P and Hierlemann A 2005 Impedance characterization and modeling of electrodes for biomedical applications *IEEE Trans. Biomed. Eng.* **52** 1295–302

- Fujita K, Lazarovici P and Guroff G 1989 Regulation of the differentiation of PC12 pheochromocytoma cells *Environ. Health Perspect.* **80** 127–42
- Gholmieh G, Soussou W, Han M, Ahuja A, Hsiao M-C, Song D, Tanguay A R Jr and Berger T W 2006 Custom-designed high-density conformal planar multielectrode arrays for brain slice electrophysiology *J. Neurosci. Methods* **152** 116–29
- Guenther T, Kong C, Lu H, Svehla M J, Lovell N H, Ruys A and Suaning G J 2014 Pt-Al₂O₃ interfaces in cofired ceramics for use in miniaturized neuroprosthetic implants *J. Biomed. Mater. Res.* **102** 500–7
- Guenther T, Mintri A, Lim W W, Jung L H, Lehmann T, Lovell N H and Suaning G J 2011 Laser-micromachined, chip-scaled ceramic carriers for implantable neurostimulators *Proc. IEEE Engineering in Medicine and Biology Society (EMBC)* pp 1085–8
- Gunning D E, Beggs J M, Dabrowski W, Hottowy P, Kenney C J, Sher A, Litke A M and Mathieson K 2013 Dense arrays of micro-needles for recording and electrical stimulation of neural activity in acute brain slices *J. Neural Eng.* **10** 016007
- Green R A et al 2013 Integrated electrode and high density feedthrough system for chip-scale implantable devices *Biomaterials* **34** 6109–18
- Green R A, Hassarati R T, Bouchinet L, Lee C S, Cheong G L M, Yu J F, Dodds C W, Suaning G J, Poole-Warren L A and Lovell N H 2012b Substrate dependent stability of conducting polymer coatings on medical electrodes *Biomaterials* **33** 5875–86
- Green R A, Matteucci P B, Dodds C W D, Palmer J, Dueck W F, Hassarati R T, Byrnes-Preston P J, Lovell N H and Suaning G J 2014 Laser patterning of platinum electrodes for safe neurostimulation *J. Neural Eng.* **11** 056017
- Green R A, Toor H, Dodds C and Lovell N H 2012a Variation in performance of platinum electrodes with size and surface roughness *Sensors Mater.* **24** 165–80
- Grumet A E, Wyatt J L Jr and Rizzo J F III 2000 Multi-electrode stimulation and recording in the isolated retina *J. Neurosci. Methods* **101** 31–42
- Hascup E R, af Bjerkén S, Hascup K N, Pomerleau F, Huettl P, Strömberg I and Gerhardt G A 2009 Histological studies of the effects of chronic implantation of ceramic-based microelectrode arrays and microdialysis probes in rat prefrontal cortex *Brain Res.* **1291** 12–20
- Henle C, Meier W, Schuettler M, Boretius T and Stieglitz T 2009 Electrical characterization of platinum, stainless steel and platinum/iridium as electrode materials for a new neural interface *World Congress on Medical Physics and Biomedical Engineering* ed O Dössel and W C Schlegel (7–12 September 2009, Munich, Germany) (Berlin: Springer) pp 100–3
- Heuschkel M O, Fejtl M, Raggenbass M, Bertrand D and Renaud P 2002 A three-dimensional multi-electrode array for multi-site stimulation and recording in acute brain slices *J. Neurosci. Methods* **114** 135–48
- Hochberg L R et al 2012 Reach and grasp by people with tetraplegia using a neurally controlled robotic arm *Nature* **485** 372–5
- ISO 10993-5:2009 2009 *Biological Evaluation of Medical Devices. Tests for in vitro Cytotoxicity* (Brussels: International Organisation for Standardization)
- ISO 10993-12:2012 2012 *Biological Evaluation of Medical Devices. Sample Preparation and Reference Materials* (Brussels: International Organisation for Standardization)
- Istamboulie G, Sikora T, Jubete E, Ochoteco E, Marty J-L and Nogueur T 2010 Screen-printed poly(3,4-ethylenedioxythiophene) (PEDOT): a new electrochemical mediator for acetylcholinesterase-based biosensors *Talanta* **82** 957–61
- Joshi K A, Tang J, Haddon R, Wang J, Chen W and Mulchandani A 2005 A disposable biosensor for organophosphorus nerve agents based on carbon nanotubes modified thick film strip electrode *Electroanalysis* **17** 54–8
- Khodagholy D, Gelinis J N, Thesen T, Doyle W, Devinsky O, Malliaras G G and Buzsáki G 2015 NeuroGrid: recording action potentials from the surface of the brain *Nat. Neurosci.* **18** 310–5
- Kumsa D W, Bhadra N, Hudak E M, Kelley S C, Untereker D F and Mortimer J T 2016 Electron transfer processes occurring on platinum neural stimulating electrodes: a tutorial on the i(Ve) profile *J. Neural Eng.* **13** 052001
- Lonys L, Vanhoestenbergh A, Julémont N, Godet S, Delplancke M-P, Mathys P and Nonclercq A 2015 Silicone rubber encapsulation for an endoscopically implantable gastrostimulator *Med. Biol. Eng. Comput.* **53** 319–29
- Miller E M, Quintero J E, Pomerleau F, Huettl P, Gerhardt G A and Glaser P E A 2015 Simultaneous glutamate recordings in the frontal cortex network with multisite biomorphic microelectrodes: new tools for ADHD research *J. Neurosci. Methods* **252** 75–9
- Moxon K A, Leiser S C, Gerhardt G A, Barbee K A and Chapin J K 2004 Ceramic-based multisite electrode arrays for chronic single-neuron recording *IEEE Trans. Biomed. Eng.* **51** 647–56
- Nam Y, Wheeler B C and Heuschkel M O 2006 Neural recording and stimulation of dissociated hippocampal cultures using microfabricated three-dimensional tip electrode array *J. Neurosci. Methods* **155** 296–99
- Newbold C, Richardson R, Millard R, Huang C, Milojevic D, Shepherd R and Cowan R 2010 Changes in biphasic electrode impedance with protein adsorption and cell growth *J. Neural Eng.* **7** 056011
- Ordóñez J, Jeschke C, Guenther T, Stieglitz T and Suaning G J 2009 Laser-structuring of thick-film conductors and its application on an optical stimulator *Proc. 14th Ann. Conf. IFESS*
- Pace S J and Hamerslag J D 1992 Thick-film multilayer ion sensors for biomedical applications *Biosensors and Chemical Sensors (American Chemical Society)* vol 487 pp 261–73
- Palanker D, Vankov A, Huie P and Baccus S 2005 Design of a high-resolution optoelectronic retinal prosthesis *J. Neural Eng.* **2** S105
- Shannon R V 1992 A model of safe levels for electrical stimulation *IEEE Trans. Biomed. Eng.* **39** 424–6
- Spira M E and Hai A 2013 Multi-electrode array technologies for neuroscience and cardiology *Nat. Nanotechnol.* **8** 83–94
- Rios G, Lubenov E V, Chi D, Roukes M L and Siapas A G 2016 Nanofabricated neural probes for dense 3D recordings of brain activity *Nano Lett.* **16** 6857–62
- Rishal I, Golani O, Rajman M, Costa B, Ben-Yaakov K, Schoenmann Z, Yaron A, Basri R, Fainzilber M and Galun M 2013 WIS-NeuroMath enables versatile high throughput analyses of neuronal processes *Dev. Neurobiol.* **73** 247–56
- Robblee L S, McHardy J, Marston J M and Brummer S B 1980 Electrical stimulation with Pt electrodes. V. The effect of protein on Pt dissolution *Biomaterials* **1** 135–9
- Rose T L and Robblee L S 1990 Electrical stimulation with Pt electrodes. VIII. Electrochemically safe charge injection limits with 0.2 ms pulses (neuronal application) *IEEE Trans. Biomed. Eng.* **37** 1118–20
- Rugheimer L, Hansell P and Wolgast M 2008 Determination of the charge of the plasma proteins and consequent Donnan equilibrium across the capillary barriers in the rat microvasculature *Acta Physiol.* **194** 335–9
- Sachs H G, Schanze T, Wilms M, Rentzos A, Brunner U, Gekeler F and Hesse L 2004 Subretinal implantation and testing of polyimide film electrodes in cats *Graefes Arch. Clin. Exp. Ophthalmol.* **243** 464–8
- Sekirnjak C, Hottowy P, Sher A, Dabrowski W, Litke A M and Chichilnisky E J 2008 High-resolution electrical stimulation of primate retina for epiretinal implant design *J. Neurosci.* **28** 4446–56

- Sorkin R, Greenbaum A, David-Pur M, Anava S, Ayali A, Ben-Jacob E and Hanein Y 2009 Process entanglement as a neuronal anchorage mechanism to rough surfaces *Nanotechnology* **20** 015101
- Steele J G, Dalton B A, Johnson G and Underwood P A 1995 Adsorption of fibronectin and vitronectin onto Primaria™ and tissue culture polystyrene and relationship to the mechanism of initial attachment of human vein endothelial cells and BHK-21 fibroblasts *Biomaterials* **16** 1057–67
- Suaning G J, Schuettler M, Ordonez J S and Lovell N H 2007 Fabrication of multi-layer, high-density micro-electrode arrays for neural stimulation and bio-signal recording *3rd Int. IEEE/EMBS Conf. on Neural Engineering, 2007. CNE '07* pp 5–8
- Vanhoestenbergh A, Musick K M, Lacour S P and Donaldson N 2012 An interconnection method for ultra-compliant electrodes *17th Annual Int. FES Society Conf.*
- Viventi J et al 2011 Flexible, foldable, actively multiplexed, high-density electrode array for mapping brain activity *in vivo* *Nat. Neurosci.* **14** 1599–605
- Wang J, Pamidi P V and Rogers K R 1998 Sol-gel-derived thick-film amperometric immunosensors *Anal. Chem.* **70** 1171–5
- Waziri A, Schevon C A, Cappell J, Emerson R G, McKhann G M and Goodman R R 2009 Initial surgical experience with a dense cortical microarray in epileptic patients undergoing craniotomy for subdural electrode implantation *Neurosurgery* **64** 540–5
- Wilson C J, Clegg R E, Leavesley D I and Percy M J 2005 Mediation of biomaterial-cell interactions by adsorbed proteins: a review *Tissue Eng.* **11** 1–18
- Wong Y T, Chen S C, Seo J M, Morley J W, Lovell N H and Suaning G J 2009 Focal activation of the feline retina via a suprachoroidal electrode array *Vis. Res.* **49** 825–33
- Zeng F, Rebscher S, Harrison W V, Sun X and Feng H 2009 Cochlear implants *Implantable neural prostheses 1: Devices and Applications* ed D Zhou and E Greenbaum (New York: Springer) pp 85–116